

# VLT spectroscopy of the Black Hole Candidate Swift J1357.2-0933 in Quiescence

M.A.P. Torres<sup>1,2,3\*</sup>, P.G. Jonker<sup>1,2</sup>, J. C. A. Miller-Jones<sup>4</sup>, D. Steeghs<sup>5</sup>, S. Repetto<sup>2</sup>, J. Wu<sup>6</sup>

<sup>1</sup>*SRON, Netherlands Institute for Space Research, Sorbonnelaan 2, 3584 CA, Utrecht, The Netherlands*

<sup>2</sup>*Department of Astrophysics/ IMAPP, Radboud University Nijmegen, Heyendaalseweg 135, 6525 AJ, Nijmegen, The Netherlands*

<sup>3</sup>*European Southern Observatory, Alonso de Córdova 3107, Vitacura, Casilla 19001, Santiago de Chile, Chile*

<sup>4</sup>*International Centre for Radio Astronomy Research, Curtin University, GPO Box U1987, Perth, WA 6845, Australia*

<sup>5</sup>*Department of Physics, University of Warwick, Coventry CV4 7AL, UK*

<sup>6</sup>*Harvard-Smithsonian Center for Astrophysics, 60 Garden Street, Cambridge, MA 02138, U.S.A.*

11 September 2021

## ABSTRACT

We present time-resolved optical spectroscopy of the counterpart to the high-inclination black hole low-mass X-ray binary Swift J1357.2-0933 in quiescence. Absorption features from the mass donor star were not detected. Instead the spectra display prominent broad double-peaked  $H\alpha$  emission and weaker  $HeI$  emission lines. From the  $H\alpha$  peak-to-peak separation we constrain the radial velocity semi-amplitude of the donor star to  $K_2 > 789 \text{ km s}^{-1}$ . Further analysis through radial velocity and equivalent width measurements indicates that the  $H\alpha$  line is free of variability due to S-wave components or disc eclipses. From our data and previous observations during outburst, we conclude that long-term radial velocity changes ascribed to a precessing disc were of low amplitude or not present. This implies that the centroid position of the line should closely represent the systemic radial velocity,  $\gamma$ . Using the derived  $\gamma = -150 \text{ km s}^{-1}$  and the best available limits on the source distance, we infer that the black hole is moving towards the Plane in its current Galactic orbit unless the proper motion is substantial. Finally, the depth of the central absorption in the double peaked profiles adds support for Swift J1357.2-0933 as a high-inclination system. On the other hand, we argue that the low hydrogen column density inferred from X-ray fitting suggests that the system is not seen edge-on.

**Key words:** binaries: close; accretion, accretion discs; X-rays: binaries; black hole physics; stars: individual: Swift J1357.2-0933

## 1 INTRODUCTION

The X-ray transient Swift J1357.2-0933 (hereafter J1357.2) was discovered in outburst on 28 Jan 2011 with the Burst Alert Telescope on-board *Swift* (Krimm et al. 2011a). Follow-up observations with the *Swift* X-ray Telescope revealed a spectrum consistent with an absorbed power law with a low hydrogen column density  $N_H$  of  $(1.2 \pm 0.7) \times 10^{20} \text{ cm}^{-2}$  and a photon index that evolved from  $\Gamma = 1.5$  to 2.1 during the outburst decline (Krimm et al. 2011b, Armas Padilla et al. 2013). A 0.5-10 keV outburst peak luminosity of  $1.1 \times 10^{35} \times (\frac{d}{1.5 \text{ kpc}})^2 \text{ erg s}^{-1}$  is inferred from these observations. In addition, XMM-Newton data obtained on 5

Feb 2011 could be fitted with a three component model: the above mentioned power law with a 93 percent contribution to the total flux, a thermal (disc) component with  $kT = 0.2 \text{ keV}$ , and one edge at 0.73 keV. The thermal component is interpreted as soft emission originating in the accretion disc, while the edge is associated to interstellar iron. The low X-ray peak luminosity together with the evolution (softening) of the power-law dominated spectrum, the low temperature for the thermal component associated to the accretion disc and the detection of radio emission (Sivakoff, Miller-Jones & Krimm 2011) are in accordance with the source being a black hole system in the low-hard state through the entire outburst. In this regard, timing analysis of both the XMM-Newton data as well as contemporaneous RXTE Proportional Counter Array observations showed a power spec-

\* email : M.Torres@sron.nl

trum with characteristics more similar to those detected in the low-hard state of black holes than neutron stars (Armas Padilla et al. 2014a). On the other hand, early in the outburst a 6 mHz quasi-periodic oscillation was detected in one of the RXTE observations. This low frequency is atypical in black holes and more common in dipping neutron stars (see Armas Padilla et al. 2014a for details).

J1357.2 was observed in quiescence with XMM-Newton on 10 July 2013 and detected at a 0.5 - 10 keV X-ray luminosity of  $8.5_{-2.6}^{+5.5} \times 10^{29} \times (\frac{d}{1.5 \text{ kpc}})^2 \text{ erg s}^{-1}$  (Armas Padilla et al. 2014b). The X-ray spectrum in quiescence is consistent with an absorbed power law with  $\Gamma = 2.1 \pm 0.4$ , although fits to single thermal models were also permitted by the data.

The optical and near-infrared counterparts to J1357.2 were identified with a  $r' \simeq 16.30$  and  $K = 17.4 \text{ mag star}^1$  (Rau et al. 2011). A high-resolution optical spectrum obtained on 2 February 2011 showed no clear indication for emission lines, lack of diffuse interstellar bands and the presence of weak absorption lines from the interstellar Na doublet (Torres et al. 2011). A low-resolution spectrum taken one day later exhibited weak and broad H $\alpha$  and H $\beta$  emission lines with the former having 7 Å equivalent width (EW) and  $\sim 4000 \text{ km s}^{-1}$  Full Width at Zero Intensity (FWZI; Milisavljevic et al. 2011). High-resolution H $\alpha$  spectroscopy undertaken on 25-27 February 2011 resolved the very broad double-peaked line profile with a peak-to-peak separation of  $\sim 1800 \text{ km s}^{-1}$  (Casares et al. 2011). Further time-resolved observations allowed Corral-Santana et al. (2013) to find a  $2.8 \pm 0.3 \text{ hr}$  modulation in radial velocities extracted from the H $\alpha$  line profile. Assuming this periodicity corresponds to the orbital period and using the line peak-to-peak separation to constrain the radial velocity semi-amplitude of the donor star to  $K_2 \geq 690 \text{ km s}^{-1}$ , a mass larger than 3.0  $M_{\odot}$  is estimated for the compact object. Complementary time-resolved optical photometry did not show any evidence for variability with the above periodicity (Corral-Santana et al. 2013). The light curves show dipping variability with a recurrence time that gradually increases from 2.3 min to 7.5 min over 69 days of follow-up photometry. The recurrent optical dips (up to 0.8 mag) are interpreted as obscuration events caused by a toroidal structure with asymmetric height with respect to the orbital plane. In this scenario, the changes in the dipping frequency would imply that this structure is moving inside-out the disc during outburst. In order to produce the profound dips in the light curve, a very large system inclination is necessary. However, neither the optical data nor the X-ray data showed dips or eclipses due to the donor star (Armas-Padilla 2013a, Corral-Santana et al. 2013). To explain the non detection of these features in the light curve, Corral-Santana et al. (2013) invoke an accreting binary configuration in which the mass ratio is low enough to have a Roche-lobe filling donor star with a radius smaller or similar to the disc outer rim.

The optical counterpart to J1357.2 was also identified in quiescence at  $r = 21.96$  in Sloan Digital Sky Survey (SDSS) images taken in May 2006 (Rau et al. 2011). Based on the SDSS pre-outburst colors and assuming no disc contribution

to the optical light, the donor star was tentatively classified as an M4 dwarf at  $\sim 1.5 \text{ kpc}$  distance. This is in good agreement with the M4.5 donor at  $\sim 1.6 \text{ kpc}$  expected from a Roche-lobe filling donor in a 2.8 hr orbital period system (Corral-Santana et al. 2013). However, time-resolved photometry during quiescence at different post-outburst epochs (Shahbaz et al. 2013) reveals a very different picture: the donor star is not the dominant source of light at optical or infrared wavelengths. The multicolor light curves lack evidence of any orbital variability caused by the donor star, i.e. ellipsoidal modulations, eclipses or dip features. Instead the photometry shows flares of up to  $\sim 1.5 \text{ mag}$  and  $\sim 2 \text{ mag}$  at optical and infrared wavelengths, respectively. This is the largest flare amplitude known in quiescent black hole X-ray binaries. Moreover, the dipping behaviour observed in outburst persists in quiescence but with a  $\sim 30 \text{ min}$  recurrence time. Both the optical to mid-infrared quiescent spectral energy distribution (SED) and optical variability SED of J1357.2 can be described by a single power-law model with index  $\Gamma \sim 1.4$ . This steep power-law together with the high amplitude flickering are interpreted as due to synchrotron emission from a variable, weak jet that dominates the SED over the donor star light (Shahbaz et al. 2013). Using the relation between orbital period and the outburst optical amplitude, Shahbaz et al. constrain the distance towards J1357.2 to be between 0.5 and 6.3 kpc.

The lack of accurate dynamical parameters and observational details of the accretion disc structure during quiescence motivated us to perform time-resolved optical spectroscopy. We begin with a description of the observations and data reduction steps (Section 2). The average optical spectrum of J1357.2 in quiescence is presented in Section 3 where we also characterize the H $\alpha$  line profile and constrain its variability. Finally, the results are presented and discussed in Section 4, where we examine key questions such as the orbital parameters and space velocity for the system. Our conclusions are summarized in Section 5.

## 2 OBSERVATIONS AND DATA REDUCTION

Time-resolved optical spectroscopy of J1357.2 was obtained with the FOcal Reducer and low dispersion Spectrograph 2 (FOR2, Appenzeller et al. 1998) which is mounted on the Cassegrain focus of the 8.2-m ESO Unit 1 Very Large Telescope at Paranal, Chile. The observations were obtained in service mode under program 091.D-0865(A) during 14 April 2013 5:37 - 6:22 UT, 18 April 2013 4:35 - 8:00 UT and 4 May 2013 4:12 - 4:57 UT. FOR2 was used with the standard resolution collimator and the 2048  $\times$  4096 pixels MIT two CCDs mosaic detector binned 2  $\times$  2 to provide a  $0''.25 \text{ pixel}^{-1}$  scale. The instrument was operated in long-slit mode with the 600 line  $\text{mm}^{-1}$  grism GRIS\_600RI. J1357.2 was centered in a  $1''.0$  wide slit with its location offset from the CCD center. This instrumental setup yields a dispersion of  $1.6 \text{ \AA pixel}^{-1}$ , a coverage in the spectral range  $\lambda\lambda 5300\text{--}8630$  and a slitwidth-limited resolution of  $\sim 5 \text{ \AA}$  full-width half maximum (FWHM). A total of six one hour-long observing blocks (OBs) were executed consisting of four spectroscopic integrations of 640 s each. Four, sixteen and four spectra were collected on 14 April at sec  $z < 1.08$ , 18 April from sec  $z 1.04$  to 1.43 and 4 May at sec  $z < 1.07$ , respectively.

<sup>1</sup> The coordinates in Rau et al. (2011) are incorrect due to a typographical error. The coordinates for J1357.2 are  $\alpha(J2000) = 13:57:16.829$  and  $\delta(J2000) = -09:32:38.75$  as provided by SDSS

We measure from the width of the source spatial profile at spectral positions covering  $H\alpha$  an image quality between  $0''.6 - 0''.8$ ,  $0''.5 - 0''.7$  and  $0''.7 - 0''.8$  for the first, second and third nights, respectively and a mean  $0''.66 \pm 0''.07$  FWHM from the three nights. Therefore the observations were obtained in seeing-limited conditions yielding a spectral resolution of  $\sim 3 \text{ \AA}$  FWHM corresponding to  $140 \text{ km s}^{-1}$  at  $H\alpha$ .

The spectra were reduced and extracted using standard techniques implemented in the STARLINK, FIGARO, and PAMELA packages while the wavelength calibration was done with MOLLY. The data reduction consisted of de-biasing and flat-fielding the data. The spectra were extracted using the algorithm of Horne (1986) to optimize the signal-to-noise ratio of the resulting spectra. Exposures using comparison arc lamps were performed after the end of each night in order to establish the pixel-to-wavelength scale. This was derived through polynomial fits to 27 arc lines. The rms scatter of the fit was always  $< 0.07 \text{ \AA}$ , which is less than  $1/22$  of the wavelength dispersion. The sky [OI]  $\lambda\lambda 5577.34, 6300.3$  lines and the OH emission blend at  $7316.3 \text{ \AA}$  showed that wavelength zeropoint disparities reached up to  $\lesssim 30 \text{ km s}^{-1}$  in amplitude. These deviations were corrected for by applying to the spectra zeropoint shifts calculated using the [OI]  $\lambda 6300.3$  emission feature. The resulting 24 spectra were normalized by dividing each of them by a low-order spline fit to the continuum after masking out emission lines and atmospheric absorption bands. Finally, the resulting spectra were rebinned to a uniform pixel scale.

Since all the observations were seeing limited, systematic effects due to excursions of the target position with respect to the slit centre may affect the radial velocity determinations presented in this work. In this regard, J1357.2 was centered on the slit at the start of each OB execution, except perhaps during the last two OBs on 18 April. For these OBs we lack the re-acquisition and through-slit images commonly saved when the centering is checked or performed during service mode observations. In what follows we will conservatively assume that for both OBs the centering step was skipped. Hence, positional departures from the exact slit center and changes in the target position during the spectroscopic exposures have certainly happened. Unfortunately we lack the data required to quantify and correct for this effect (see e. g. Bassa et al. 2006). Section 2.4.3 in the ESO FORS2 manual (Issue 92.0) offers constraints on the image motion for a given  $z$  due to instrument flexures. This motion increases with  $z$ . As our observations were performed after culmination,  $z$  increased monotonously and it is therefore reasonable to assume that the offsets in the target position accumulate. Thus, we estimate a cumulative offset  $< 0.3$  (binned) pixels at the end of the execution of the single OBs during 14 April and 4 May. The cumulative offsets at the end of the four OBs executed on 18 April are estimated to be  $< 0.3, < 0.3, < 0.7, < 1.1$  binned pixels. The systematic effects could therefore have introduced radial velocity offsets (at  $H\alpha$ ) from  $< 22$  to  $< 84 \text{ km s}^{-1}$ . We have measured the positional offsets along the spatial direction. For this we have calculated the centroid for the spatial profile of J1357.2 at  $H\alpha$  in all spectra. The centroids differ by  $< 0.3$  (binned) pixels. This suggests that the cumulative positional offsets in the dispersion direction during 18 April may

be smaller than estimated if they have a similar amplitude to that measured for the offsets in the spatial direction.

### 3 DATA ANALYSIS

#### 3.1 Averaged spectral features

In Fig. 1, we present the result obtained by averaging the 24 individual FORS2 spectra. The averaged data show no evidence for photospheric features from the donor star such as the TiO bands characteristic of M-type stars. The interstellar sodium doublet found in outburst by Torres et al. (2011) is not obvious due to the low reddening towards the source and the fact that this feature falls on top of the He I  $\lambda 5876$  emission line. All significant absorption features in the spectrum are caused by the Earth's atmosphere. The spectrum is dominated by a prominent broad and double-peaked  $H\alpha$  emission line together with weaker emission lines of He I  $\lambda\lambda 5876, 6678, 7065$ . He I  $\lambda 5876$  is also double-peaked while He I  $\lambda 6678$  is partially resolved from the  $H\alpha$  line red wing. At red wavelengths there is no obvious emission from Paschen lines or the two Ca II triplet components covered by the data. The apparent emission feature at  $\sim \lambda 8492 - 3$  is not coincident with any of the above Hydrogen or Ca II lines and it is most likely an artifact.

The mean  $H\alpha$  and He I  $\lambda 5876$  double-peaked line profiles were fitted with 1 and 2-Gaussian functions using the Marquardt algorithm (Bevington 1969). From the 1-Gaussian fit we derive the line FWHM given in Table 1. The 2-Gaussian model allows us to measure the velocity shifts of the blue ( $V_b$ ) and red ( $V_r$ ) peaks with respect to the line rest wavelength. Their difference  $\Delta V^{pp} = V_r - V_b$  (peak-to-peak separation) and mean  $(V_r + V_b)/2$  (centroid of the line) are included in Table 1. This Table also lists the measured full-width at zero intensity (FWZI) and equivalent widths (EWs) for  $H\alpha$  and He I  $\lambda\lambda 5876, 7065$ . The mean FWHM for  $H\alpha$  is consistent with the  $\sim 3900 \text{ km s}^{-1}$  FWHM found for this line in low-resolution spectroscopy obtained on 29 April 2013 UT (Shahbaz et al. 2013), although on that occasion the line profile appeared single peaked and with  $-120 \text{ \AA}$  EW. This value is below the maximum EW observed when studying the time variability of  $H\alpha$  (Section 3.2).

The mean peak-to-peak velocity separations for the  $H\alpha$  and He I  $\lambda 5876$  lines are  $2340 \pm 20 \text{ km s}^{-1}$  and  $2640 \pm 70 \text{ km s}^{-1}$ , respectively. This difference suggests that the He I emission line originates from regions in the disc closer to the black hole than the regions responsible for the  $H\alpha$  emission. The FWHM and velocity separation of the double peaks in the  $H\alpha$  line (Table 1) are a factor 1.2-1.3 larger than the values reported during outburst ( $\sim 3300 \text{ km s}^{-1}$  FWHM and  $\Delta V^{pp} = 1790 \pm 67 \text{ km s}^{-1}$ , Corral-Santana et al. 2013). This difference is expected for a disc with a Keplerian velocity field since during outburst the disc increases its radius, thereby decreasing the velocity of the outer disc regions. The  $\sim 138 \text{ \AA}$  FWZI of the  $H\alpha$  and He I  $\lambda 5876$  implies projected velocities  $\gtrsim 3150$  and  $\gtrsim 3520 \text{ km s}^{-1}$  for the inner part of the accretion disc emitting at these wavelengths. The FWZI found for  $H\alpha$  is a factor  $\sim 1.6$  larger than observed at different times during the outburst (Milisavljevic et al. 2011, see also fig. 1 in Corral-Santana et al. 2013). This difference in FWZI can be explained if the luminosity of the continuum

decreased quicker than the luminosity of the emission lines when the source went from outburst to quiescence.

### 3.2 H $\alpha$ line profile time variability

We studied the variability of the H $\alpha$  line with diverse methods. These included single and 2-Gaussian model fitting, the double-Gaussian technique described by Shafter et al. (1986) and line EW measurements. The results obtained from these techniques are shown in Fig. 2. A single Gaussian fit to the line profiles yields radial velocities ranging from -189 to +118 km s<sup>-1</sup>. These radial velocities reflect variations in the peak-to-peak intensities rather than changes in the line centroid (see below). The change in the double-peak intensity from almost symmetric peaks to enhanced red-shifted or blue-shifted peaks is obvious in Fig. 3 where we show the line profiles. Even though this behavior could be naively attributable to an S-wave originating in a hot spot and/or the donor star, further inspection of the individual data in Fig. 3 shows that the presence of such a narrow component is not obvious. In addition, these variations in the profile structure can also not be explained as due to the eclipse of the accretion disc by the donor star. In such a scenario the blue-shifted disc emission is first eclipsed while the red-shifted emission is eclipsed afterwards since the donor star initially occults disc regions moving towards the observer and subsequently blocks the receding regions from view. This is a distinctive rotational disturbance of the line profiles during eclipse, the so-called Z-wave. Thus the changes in the H $\alpha$  line profile of J1357.2 do not show the Z-wave characteristic of emission line eclipses. The variations in the peak intensities are likely due to a highly variable non-uniform disc brightness distribution or/and departures from an axisymmetric flat disc. In this regard, we observe changes of up to 10 percent in the peak-to-peak separation over successive spectra (see below). The short-term (sub-orbital) changes in the H $\alpha$  line profile morphology are reminiscent of those observed in the black hole low-mass X-ray binary (LMXB) GRO J0422+32 ( $P_{orb} = 5.1$  hr,  $q=0.12$ ) in quiescence (see fig. 1 in Filippenko et al. 1995). Another variable feature in the line shape is the depth of the central absorption delimited by the two line peaks. While the averaged line profile shows a moderately deep absorption, the individual spectra reveal that its depth can vary significantly during consecutive spectra. As observed in the first night (top-left panel Fig.3), the absorption core passes from being near the continuum level in the first spectrum to well above the continuum in the next one. Such deep cores are expected from discs observed at high inclination (see discussion).

Radial velocities were also derived with the double-Gaussian technique (Shafter et al. 1986) which consists of convolving the line profiles with two Gaussian bandpasses with separation  $a$ . After several trials, we chose to use a 200 km s<sup>-1</sup> FWHM for both Gaussians. The separation  $a$  between the Gaussians was varied from 2300 km s<sup>-1</sup> to 6000 km s<sup>-1</sup> in steps of 100 km s<sup>-1</sup>. The radial velocity curves obtained with Gaussian separations  $a \sim 2700 - 3200$  km s<sup>-1</sup> displayed a modulation with a higher amplitude than found in the radial velocities determined with a 1-Gaussian fit. We display in Fig. 2 the results for a Gaussian separation of 2800 km s<sup>-1</sup>. At Gaussian separations larger than 3300 km s<sup>-1</sup>, the radial velocities obtained with the double-Gaussian tech-

nique show no obvious modulation. Ideally the wings of disc emission lines should trace the motion of the compact object. In fact, by applying the above technique to their outburst data, Corral-Santana et al. (2013) recovered radial velocity modulations beyond  $a = 3300$  km s<sup>-1</sup> - note here that the H $\alpha$  line profile was narrower during outburst. In this way they were able to estimate the orbital period and the radial velocity semi-amplitude of the primary ( $K_1 = 43 \pm 2$  km s<sup>-1</sup>) for J1357.2. Our failure to do this could be primarily due to the systematic effects affecting the radial velocities (Section 2). The systematic velocity shifts could be comparable to or larger than  $K_1$ . Additionally, systematic effects are expected due to contamination of the red line wing by the overlapping He I  $\lambda 6678$  emission line.

The 2-Gaussian model was employed to calculate both the peak-to-peak separation and the line centroid. The changes in the line morphology from near-symmetric to asymmetric double-peaked velocity profiles were taken into consideration when calculating these parameters. This was done because the Gaussian component accounting for the weaker peak in the line will fit also part of the broader base of the profile. This yields a velocity that could be significantly offset from the real peak position in question. To avoid this possible bias effect we examined each individual fit and rejected from our analysis  $V_b$  and  $V_r$  when either of the related Gaussian components had  $FWHM > 45$  km s<sup>-1</sup>. This limit proved to be an effective quantitative way to select strongly (eight in total) asymmetric profiles - for comparison the FWHMs of the 2-Gaussians fit to the mean profile in section 3.1 is  $\sim 35$  km s<sup>-1</sup>. Note also that this non-physical two component model yields reduced  $\chi^2 = 1.0$  to 1.4, providing therefore statistically sound fits. By using profiles for which both Gaussian components have  $FWHM < 45$  km s<sup>-1</sup> (16 spectra), we derive a mean peak-to-peak separation of  $\overline{V_r - V_b} = 2370 \pm 70$  km s<sup>-1</sup> and centroid of  $(\overline{V_r + V_b})/2 = -130 \pm 60$  km s<sup>-1</sup>. The uncertainties here and below correspond to the rms scatter. We also calculated the above line parameters by including velocity shifts obtained from the asymmetric profiles. For these profiles only one of the 2-Gaussian components in the fit is narrow ( $< 45$  km s<sup>-1</sup> FWHM) yielding  $V_b$  (7 spectra) or  $V_r$  (1 spectrum). Taking the mean of all the reliable velocity shifts ( $\overline{V_b}, \overline{V_r}$ ), we derive  $\overline{V_r - V_b} = (1060 \pm 50) - (-1325 \pm 80) = 2390 \pm 100$  km s<sup>-1</sup> and  $\overline{V_r + V_b}/2 = -130 \pm 50$  km s<sup>-1</sup>. The results from both calculations are fully consistent. The temporal variability for these two line parameters derived from the 2-Gaussian model fitting is also displayed in Fig. 2 (top and middle panels). On 18 April the line centroid shows no clear modulation with velocities ranging from -222 km s<sup>-1</sup> to -50 km s<sup>-1</sup>. The amplitude of the variations is lower than that obtained from velocities derived with the 1-Gaussian model (300 km s<sup>-1</sup> amplitude) and double-Gaussian technique (650 km s<sup>-1</sup>). On 4 May the line centroid is constant during the 45 min length of the observations with a mean value of  $-180 \pm 6$  km s<sup>-1</sup>. During the three nights the peak-to-peak separation ranges from 2200 to 2530 km s<sup>-1</sup>. Variations in the peak-to-peak separation can occur in short intervals as observed on 14 April and 5 May when in a  $\sim 20$  min interval changes of  $130 \pm 50$  and  $200 \pm 60$  km s<sup>-1</sup> in amplitude take place. The fast changes (sub-orbital) in the peak-to-peak separation and intensities indicate that there are azimuthal variations in the outer disc velocities or structures.

The H $\alpha$  EW varies irregularly as shown in the bottom of Fig. 2. With our 640s integration, the EW ranges values from  $-73$  to  $-129$  Å with a mean of  $-100 \pm 14$  Å. The 14 April EW curve lacks any evidence for a decrease or increase in the line EW due to eclipses of the disc by the donor star. A decrease in the EW would occur at and near mid-eclipse if the disc regions responsible for the continuum and line are obscured from view by the donor star. On the other hand, an increase in EW can be associated with emission line regions in the disc that are not tightly confined to the orbital plane and thereby visible during eclipse. Examples of the increase in the H $\alpha$  EW at eclipse time can be found in the neutron star LMXB sources X1822-371 ( $P_{orb} = 5.1$  hr; Harlaftis et al. 1982) and EXO 0748-676 ( $P_{orb} = 3.8$  hr; Pearson et al. 2006). None of these characteristics are present in the EW curve which appears dominated by erratic variations. For comparison with other black hole LMXBs in quiescence, the strength of H $\alpha$  is not above than that found in GRO J0422+32 ( $-181$  to  $-214$  Å; Harlaftis et al. 1999).

### 3.3 Further analysis: cross-correlation and H $\alpha$ Doppler tomography

In order to search for signatures of the donor star that could have been canceled out by averaging the data, we cross-correlated the individual spectra against SDSS stellar templates covering spectral types between F and M. The cross-correlation was performed over sections free of telluric and emission line features. No cross-correlation functions were discernable from this analysis.

In an attempt to corroborate the 2.8 hr orbital period, we performed Doppler tomography on the H $\alpha$  line by phase folding the data over different trial periods and adopting a systemic radial velocity of  $-150$  km s $^{-1}$  (see Section 4.2). The tomograms (not shown) lead to variable asymmetries in the disc emission, but not to the extent that there was a clear favoured period. The reason why we were unable to use the tomographic reconstruction to constrain the orbital period is the lack of an S-wave that would have resulted in a strong emission feature in the tomogram.

## 4 DISCUSSION

Our optical spectroscopy of J1357.2 during quiescence shows no evidence for absorption features from the donor star. We therefore make use of the strong double-peaked H $\alpha$  emission line to set constraints on the system parameters. For this, comparison will be drawn between the spectroscopic and photometric properties of J1357.2 and those observed in relevant types of accreting binaries such as accretion disc corona (ADC) systems and ultra-compact binaries with a white dwarf accretor (better known as AM CVn systems). ADC sources are persistent LMXBs with an orbital inclination of  $> 80^\circ$ . AM CVn systems have in common with short orbital period black hole LMXBs a low mass ratio  $q = M_2/M_1 \lesssim 0.1$ , where  $M_2$  and  $M_1$  are the mass of the donor star and accreting object, respectively.

### 4.1 The radial velocity semi-amplitude of the donor star

Assuming an axisymmetric disc with gas in Keplerian motion, the projected motion of the outer edge of the disc  $V_d$  can be used to constrain the radial velocity semi-amplitude of the donor star ( $K_2$ ) given that  $K_2 < V_d$ .  $V_d$  has been determined for eight black hole LMXBs in quiescence by modelling the phase averaged H $\alpha$  line profile and by locating the hotspot in Doppler tomograms (e.g. Orosz et al. 1994 and Marsh et al. 1994). In this way it has been found that  $V_d(H\alpha)/K_2$  is between 1.11 and 1.47 (table 2 in Orosz et al. 2002). Using this empirical relationship and the H $\alpha$  line observed in outburst, Corral-Santana et al. (2013) constrained  $K_2 > 716 \pm 26$  km s $^{-1}$ . For this they adopted  $V_d(H\alpha)/K_2 = 1.25$  (Orosz et al. 1994, Orosz & Bailyn 1995) and took into account that, since the source is in outburst, the peak-to-peak separation is less than  $2 \times V_d(H\alpha)$  during quiescence. Following a similar approach, we constrain  $K_2$  to be  $\gtrsim 796 \pm 7$  km s $^{-1}$  ( $K_2 > 789$  km s $^{-1}$ ) by conservatively using  $V_d(H\alpha)/K_2 \leq 1.47$  during quiescence, the observational fact that  $2 \times V_d(H\alpha) \gtrsim \Delta V^{pp}$  and  $\Delta V^{pp} = 2340 \pm 20$  km s $^{-1}$  as found from the averaged H $\alpha$  profile during quiescence (Section 3.1). This implies a mass function  $f(M_1) > 6.0 M_\odot$  if J1357.2 is in a  $2.8 \pm 0.3$  hr orbit.

Adopting the radial velocity semi-amplitude of the primary ( $K_1 = 43 \pm 2$  km s $^{-1}$ ; Corral-Santana et al. 2013) derived by applying the double-Gaussian technique to outburst data of the H $\alpha$  emission line, a constraint for the mass ratio  $q = K_1/K_2 \lesssim 0.054$  is obtained.

### 4.2 The systemic radial velocity

The characterization of the H $\alpha$  profile performed in Section 3.2 shows that its centroid is offset to the blue on average by  $130 \pm 50$  km s $^{-1}$ . The position of a line originating in a disc will be shifted from its rest wavelength by the systemic radial velocity and primary's radial velocities at the time of the observation as:  $\gamma + K_1 \sin 2\pi\phi$ , where  $\gamma$  is the systemic radial velocity and  $\phi$  is the orbital phase. Additional velocity components are usually present. They are due, for instance, to emission from the gas stream, hot spot and/or donor star. Furthermore, departures from a disc with gas in Keplerian motion are possible in LMXBs due to tidal effects on the disc. The tidal action of the donor on the outer parts of the disc can excite spiral shock patterns or cause the disc to elongate and precess. Disc precession can dominate the orbital-averaged velocity shifts observed in the emission line centroid. These contributions to the velocity profile can make it difficult to reliably establish  $\gamma$  or  $K_1$  from time-resolved spectroscopy of emission lines (see e.g. Orosz et al. 1994 and sec 7.5 in Shahbaz et al. 2013).

In what follows we present and discuss three pieces of observational evidence that indicate that the  $-130$  km s $^{-1}$  offset of the H $\alpha$  line centroid in J1357.2 most likely represents (within the errors) the systemic radial velocity: first, as reported in Section 3.2. the double-peaked H $\alpha$  line profiles lack the presence of any narrow line component with velocity position modulated with the orbital motion. Therefore, J1357.2 shows no S-wave associated to emission from confined regions in the accretion flow (as discussed above) that can produce a radial velocity offset in an averaged line

profile when the orbital phase coverage during the observations is non-uniform. S-waves are features commonly present in the time-resolved spectra of accreting binaries, but exceptions exist where this feature is not detected or is very weak. This is the case in GRO J0422+32 for which no S-wave was present in H $\alpha$  spectroscopy during quiescence (Harlaftis et al. 1999). See also Mason et al. (2001) and Levitan et al. (2011) for examples of lack of/weak S-waves in a 1.8 hr dwarf nova and in an AM CVn system, respectively. Second, the average radial velocity offset found during quiescence is fully consistent with the  $\gamma$  velocity of  $\sim -150 \text{ km s}^{-1}$  that can be derived from the diagnostic diagram for this Balmer line during outburst (fig. S2 in Corral-Santana et al. 2013). Third, Corral-Santana et al. found  $\gamma$  and a periodic (likely orbital) modulation from spectroscopic data obtained in two outburst epochs separated by  $\sim 20$  days. The detection of an orbital modulation in the combined data sets is possible if any additional velocity shifts in the line centroid on a timescale longer than the orbital period were small or if they had similar magnitude and sign at the time of the observations. For CVs and LMXBs with  $q \lesssim 1/4$ , long-term line shifts are expected during outburst due to disc eccentricity and precession. The formation of such a disc is attributed to the tidal influence of the donor star over a disc that during outburst radially expands to reaches the 3:1 resonance radius (see e.g. Hirose & Osaki 1990, Whitehurst & King 1991). The variations in the emission line centroids observed in XTE J1118+480 ( $P_{orb} = 4.08 \text{ hr}$ ,  $q=0.037$ ; Zurita et al. 2002, Torres et al. 2004) and AM Canum Venaticorum ( $P_{orb} = 17 \text{ min}$ ,  $q = 0.18$ ; Roelofs et al. 2006) provide evidence for the existence of large amplitude velocity shifts driven by a precessing disc. When present they can make it difficult to recover any orbital modulation superimposed on the lines by using data sets spanning many orbits and lacking enough orbital phase coverage at each epoch of observation. It appears therefore that long-term changes in the line centroid due to a precessing accretion disc were small or absent in J1357.2 (at least) at the time of the spectroscopic observations.

In support of the possibility of a non-precessing disc on J1357.2 is the absence of superhumps in the outburst light curves presented in Corral-Santana et al. (2013). Superhumps are photometric modulations that are driven by outbursts and characterized by having a periodicity a few percent longer than the actual orbital period. This photometric behaviour is explained as due to the presence of the elliptical and precessing disc. Superhumps have been found during the outburst decline of the short orbital period black hole LMXBs GRO J0422+32 (O’Donoghue & Charles 1996), XTE J1118+480 (Uemura et al. 2000, Zurita et al. 2002, 2006) and Swift J1753.5-0127 ( $P_{orb} = 3.2 \text{ hr}$ , Zurita et al. 2008). The apparent lack of superhumps in J1357.2 is striking, but not impossible given that these features do not necessarily develop or persist during all outbursts. A clear example is the eclipsing AM CVn system SDSS J0926+3624 ( $P_{orb} = 28 \text{ min}$ ,  $q = 0.04$ ) which exhibited superhumps in an outburst in 2006 and lacked these features in an outburst with similar brightness amplitude that occurred in 2009 (Copperwheat et al. 2011). Alternatively, the considerable dipping in the outburst light curve of J1357.2 might not have permitted the detection of the superhump signal which has been argued to be of low amplitude for high incli-

nation LMXBs (Haswell et al. 2011). However, see Mason et al. (2008) and Hakala et al. (2008) for the detection of superhumps in the ADC neutron star system MS 1603.6+2600 ( $P_{orb} = 1.9 \text{ hr}$ ).

In summary, the absence of S-wave components in the H $\alpha$  line during quiescence, the similar values of the averaged line centroid during quiescence and the  $\gamma$  measured during outburst together with the apparent lack during outburst of significant long-term changes in the line strongly support the claim that the averaged centroid of the H $\alpha$  line closely represents the systemic radial velocity of J1357.2. Since our radial velocities could have been affected to a greater or lesser degree by systematic effects (Section 2), we prefer and adopt for the rest of the discussion the value of  $\gamma \sim -150 \text{ km s}^{-1}$  derived in Corral-Santana et al. (2013).

### 4.3 The space velocity

Since the distance to J1357.2 is poorly constrained (0.5–6.3 kpc) and the proper motion is unknown, we cannot draw definitive conclusions on the space velocity of the source. Given the high Galactic latitude of J1357.2 ( $b = 50^\circ$ ) the range of possible distances implies that the source lies between 0.4 and 4.8 kpc above the Galactic Plane. With the known position and systemic radial velocity ( $-150 \text{ km s}^{-1}$ ), we can compute the Galactic space velocity components  $U$ ,  $V$  and  $W$  for a grid of possible proper motions (in both right ascension and declination) and distances, using the transformations of Johnson & Soderblom (1987). We find that the  $W$  velocity component (motion perpendicular to the Galactic plane) is directed back towards the Plane, unless the proper motions are large enough that the velocity components parallel to the plane of the disc deviate significantly (by  $> 150 \text{ km s}^{-1}$ ) from the standard Galactic rotation at  $240 \text{ km s}^{-1}$  (Reid et al. 2014). This would imply that the source was originally at an even larger distance from the Galactic Plane. Either it is a halo object, or (more likely) was formed in the disc and subsequently launched into an extremely elliptical orbit by a significant natal kick during the supernova explosion in which the black hole was formed, as also inferred to have occurred in GRO J1655-40 (Brandt, Podsiadlowski & Sigurdsson 1995) and XTE J1118+480 (Mirabel et al. 2001).

To place better constraints on the space velocity of J1357.2 would require knowledge of the source proper motion. However, since the quiescent counterpart of J1357.2 is fainter than Gaia’s limiting magnitude of  $G = 20$ , an accurate proper motion for J1357.2 would require VLBI observations, either of the (as-yet undetected) quiescent radio emission, or of future transient outbursts (e.g. Mirabel et al. 2001; Russell et al., 2015).

### 4.4 The orbital inclination

An edge-on nature for J1357.2, as proposed to explain the profound dips in the optical light curves (Corral-Santana et al. 2013) is questionable. As argued by Armas-Padilla et al. (2014a) the X-ray spectrum during outburst shows an excess of soft emission attributable to non-occulted inner regions of the accretion disc. Moreover the X-ray spectrum lacks emission/absorption X-ray features frequently observed in ADC

sources (see sec. 4.1 in Armas-Padilla et al. 2014a) or in high-inclination neutron star LMXBs (Boirin et al. 2005; Díaz Trigo & Boirin 2013). Furthermore, there is another significant difference between J1357.2 in outburst and X-ray bright high-inclination systems (not necessarily ADC sources). In addition to extinction from interstellar matter, the  $N_H$  as measured in X-ray spectral fits usually includes the absorption associated to matter local to the source. The latter can be the dominant contribution to  $N_H$  when reddening towards the source is very low. In several high-inclination systems the  $N_H$  determined from X-ray spectral fits is indeed dominated by extinction local to the source. For instance, ultraviolet observations have enabled reliable determinations of the interstellar reddening  $E(B-V)$  towards EXO 0748-676 and X2127+119 (which have  $P_{orb} = 3.8$  hr and  $P_{orb} = 17.1$  hr, respectively): for both sources  $E(B-V) \sim 0.06$  mag (Ioannou et al. 2003, Pearson et al. 2006) equivalent to  $N_H \sim 3 \times 10^{20}$  cm $^{-2}$  when using Bohlin et al. (1978)'s  $E(B-V)$  to  $N_H$  scaling. These values are much lower than  $N_H$  values found from X-ray fitting (see EXO 0748-676 Bonnet-Bidaud et al. 2001 and White & Angelini 2001 for X2127+119).

In other high-inclination sources the  $N_H$  found for dipping and/or eclipsing LMXBs when using the out-of-dips or eclipse X-ray emission is typically of the order of  $10^{21}$  cm $^{-2}$  as found for MS 1603.6+2600 ( $P_{orb} = 1.9$  hr, Hakala et al. 2005), XTE J1710-281 ( $P_{orb} = 3.8$  hr (Young et al. 2009), X1822-371 ( $P_{orb} = 5.6$  hr, Somero et al. 2012, Iaria et al. 2013), and other longer/shorter orbital-period high-inclination neutron star systems (Díaz Trigo et al. 2006).

Both the absolute value of  $N_H$  and the difference between the  $N_H$  from X-ray spectral fits and the optically-derived equivalent  $N_H$  are very low for J1357.2. *Swift* data delivered  $N_H$  of  $(1.2 \pm 0.7) \times 10^{20}$  cm $^{-2}$  while fits to XMM data could not constrain it (Krimm et al. 2011b, Armas-Padilla et al. 2013). We can use the EWs of the interstellar Na doublet found in outburst (Torres et al. 2011) to estimate the interstellar reddening towards J1357.2. The resolved Na D1 and D2 components, have  $\sim 0.3$  Å and  $\sim 0.2$  Å, respectively. We derive  $E(B-V) \sim 0.1$  from the Na D1 line EW using the calibration of Munari & Zwitter (1997) and 0.05 from the Na D2 EW assuming a D2/D1 ratio of 2 (optically thin limit). Thus  $E(B-V)$  is likely 0.05 – 0.1 and thereby  $N_H = (3 - 6) \times 10^{20}$  cm $^2$  which is very similar to the  $N_H$  derived from the X-ray spectral fits given the systematic effects in both methods employed. On the basis of this, we conclude that J1357.2 has a low  $N_H$  when compared to the value expected from a dipping and/or eclipsing high inclination LMXB. Possibly, the scale height of the material responsible for the local  $N_H$  enhancement is lower in J1357.2, or alternatively, the system inclination is lower than that of the high inclination systems we compared with. But this seems to suggest that the inclination in J1357.2 is lower than what has been suggested previously and probably  $\lesssim 80^\circ$ . This would explain the lack of disc eclipses in the continuum or H $\alpha$  lines. Nevertheless, the orbital inclination of J1357.2 cannot be too low given the observed emission line characteristics. In particular, the depth of the absorption core defined by the line peaks is similar to that observed during quiescence in eclipsing CVs (Marsh & Horne 1987) and is a strong indicator that the system has a high orbital

inclination (Horne & Marsh 1986). We conclude that the inclination of J1357.2 is probably between 70–80°.

## 5 CONCLUSIONS

Optical spectra of J1357.2 during quiescence were analyzed in this work. The average data shows a continuum lacking photospheric lines from the donor star. Thus we spectroscopically prove that synchrotron emission from a jet and/or thermal emission from the accretion disc fully veil the light contribution from the donor star at optical wavelengths. Broad strong H $\alpha$  and weaker HeI emission lines are present in the data. The time-resolved H $\alpha$  line profile shows no strong S-wave patterns or other obvious periodic behavior such as Z-wave caused by eclipses. We also find that no large long-term radial velocity shifts were present, either at the time of our spectroscopy, or of the spectroscopy acquired in outburst. Thus the data supports a systemic velocity  $\gamma = -150$  km s $^{-1}$  on the basis of the average radial velocity properties. From the H $\alpha$  peak-to-peak separation we constrain  $K_2$  to be  $\gtrsim 796 \pm 7$  km s $^{-1}$  and  $q \lesssim 0.054$ . We estimate an interstellar absorption column towards the source of  $(3 - 6) \times 10^{20}$  cm $^{-2}$  which is comparable to that derived from X-ray fitting and lower than expected from an edge-on source. Therefore the low X-ray brightness and spectral shape during outburst are unlikely due to a geometric effect (accretion disc corona system) and they are consistent with the source being in the low-hard state during the entire outburst. Although J1357.2 appears not to be one of the many missing eclipsing black-hole LMXBs, the system has high inclination as inferred from the emission line morphology. Finally, we infer that the present Galactic kinematics of J1357.2 are such that its  $W$  space velocity component is directed towards the Galactic Plane unless the proper motion is substantial.

## ACKNOWLEDGMENTS

We thank the anonymous referee for useful comments on the manuscript. We would like to thank Remco de Kok for an independent search for the cross-correlation signal from the donor star in J1357.2 and Jorge Casares for providing us with spectral templates used in these analysis. JCAMJ is the recipient of an Australian Research Council (ARC) Future Fellowship (FT140101082), and also acknowledges support from an ARC Discovery Grant (DP120102393). DS acknowledges support from STFC through an Advanced Fellowship (PP/D005914/1) as well as grant ST/I001719/1

## REFERENCES

- Appenzeller, I., Fricke, K., Fürtig, W., et al. 1998, *The Messenger*, 94, 1
- Armas Padilla, M., Degenaar, N., Russell, D. M., & Wijnands, R. 2013, *MNRAS*, 428, 3083
- Armas Padilla, M., Wijnands, R., Altamirano, D., et al. 2014a, *MNRAS*, 439, 3908
- Armas Padilla, M., Wijnands, R., Degenaar, N., et al. 2014b, *MNRAS*, 444, 902

- Bassa, C. G., van Kerkwijk, M. H., Koester, D., & Verbunt, F. 2006, *A&A*, 456, 295
- Bevington, P. R. 1969, *Data Reduction and Error Analysis for the Physical Sciences*, McGraw-Hill, New York
- Bohlin, R. C., Savage, B. D., & Drake, J. F. 1978, *ApJ*, 224, 132
- Bonnet-Bidaud, J. M., Haberl, F., Ferrando, P., Bennie, P. J., & Kendziorra, E. 2001, *A&A*, 365, L282
- Brandt, W. N., Podsiadlowski, P., & Sigurdsson, S. 1995, *MNRAS*, 277, L35
- Casares, J., Torres, M. A. P., Negueruela, I., et al. 2011, *The Astronomer's Telegram*, 3206, 1
- Copperwheat, C. M., Marsh, T. R., Littlefair, S. P., et al. 2011, *MNRAS*, 410, 1113
- Corral-Santana, J. M., Casares, J., Muñoz-Darias, T., et al. 2013, *Science*, 339, 1048
- Dehnen, W., & Binney, J. J. 1998, *MNRAS*, 298, 387
- Díaz Trigo, M., Parmar, A. N., Boirin, L., Méndez, M., & Kaastra, J. S. 2006, *A&A*, 445, 179
- Díaz Trigo, M., & Boirin, L. 2013, *Acta Polytechnica*, 53, 659
- Filippenko, A. V., Matheson, T., & Ho, L. C. 1995, *ApJ*, 455, 614
- Hakala, P., Ramsay, G., Muhli, P., et al. 2005, *MNRAS*, 356, 1133
- Hakala, P., Hjalmsdotter, L., Hannikainen, D. C., & Muhli, P. 2009, *MNRAS*, 394, 892
- Harlaftis, E. T., Charles, P. A., & Horne, K. 1997, *MNRAS*, 285, 673
- Harlaftis, E., Collier, S., Horne, K., & Filippenko, A. V. 1999, *A&A*, 341, 491
- Haswell, C. A., King, A. R., Murray, J. R., & Charles, P. A. 2001, *MNRAS*, 321, 475
- Hirose, M., & Osaki, Y. 1990, *PASJ*, 42, 135
- Horne, K., & Marsh, T. R. 1986, *MNRAS*, 218, 761
- Horne, K. 1986, *PASP*, 98, 609
- Iaria, R., Di Salvo, T., D'Ai, A., et al. 2013, *A&A*, 549, A33
- Ioannou, Z., van Zyl, L., Naylor, T., et al. 2003, *A&A*, 399, 211
- Johnson, D. R. H., & Soderblom, D. R. 1987, *AJ*, 93, 864
- Krimm, H. A., Barthelmy, S. D., Baumgartner, W., et al. 2011, *The Astronomer's Telegram*, 3138, 1
- Krimm, H. A., Kennea, J. A., & Holland, S. T. 2011a, *The Astronomer's Telegram*, 3142, 1
- Levitán, D., Fulton, B. J., Groot, P. J., et al. 2011, *ApJ*, 739, 68
- Marsh, T. R., Horne, K., & Shipman, H. L. 1987, *MNRAS*, 225, 551
- Mason, P. A., Robinson, E. L., Gray, C. L., & Hynes, R. I. 2008, *ApJ*, 685, 428
- Marsh, T. R., Robinson, E. L., & Wood, J. H. 1994, *MNRAS*, 266, 137
- Mason, E., Skidmore, W., Howell, S. B., & Mennickent, R. E. 2001, *ApJ*, 563, 351
- Milisavljevic, D., Fesen, R. A., Parrent, J. T., & Thorstensen, J. R. 2011, *The Astronomer's Telegram*, 3146, 1
- Mirabel, I. F., Dhawan, V., Mignani, R. P., Rodrigues, I., & Guglielmetti, F. 2001, *Nat*, 413, 139
- Munari, U., & Zwitter, T. 1997, *A&A*, 318, 269
- O'Donoghue, D., & Charles, P. A. 1996, *MNRAS*, 282, 191
- Orosz, J. A., Bailyn, C. D., Remillard, R. A., McClintock, J. E., & Foltz, C. B. 1994, *ApJ*, 436, 848
- Orosz, J. A., & Bailyn, C. D. 1995, *ApJ*, 446, L59
- Orosz, J. A., Groot, P. J., van der Klis, M., et al. 2002, *ApJ*, 568, 845
- Pearson, K. J., Hynes, R. I., Steeghs, D., et al. 2006, *ApJ*, 648, 1169
- Ponti, G., Fender, R. P., Begelman, M. C., et al. 2012, *MNRAS*, 422, L11
- Rau, A., Greiner, J., & Filgas, R. 2011, *The Astronomer's Telegram*, 3140, 1
- Reid, M. J., Menten, K. M., Brunthaler, A., et al. 2014, *ApJ*, 783, 130
- Roelofs, G. H. A., Groot, P. J., Nelemans, G., Marsh, T. R., & Steeghs, D. 2006, *MNRAS*, 371, 1231
- Russell et al. 2015, accepted by *MNRAS*.
- Shafter, A. W., Szkody, P., & Thorstensen, J. R. 1986, *ApJ*, 308, 765
- Shahbaz, T., Russell, D. M., Zurita, C., et al. 2013, *MNRAS*, 434, 2696
- Sivakoff, G. R., Miller-Jones, J. C. A., & Krimm, H. A. 2011, *The Astronomer's Telegram*, 3147, 1
- Somero, A., Hakala, P., Muhli, P., Charles, P., & Vilhu, O. 2012, *A&A*, 539, A111
- Torres, M. A. P., Callanan, P. J., Garcia, M. R., et al. 2002, *ApJ*, 569, 423
- Torres, M. A. P., Callanan, P. J., Garcia, M. R., et al. 2004, *ApJ*, 612, 1026
- Torres, M. A. P., Steeghs, D., Jonker, P. G., & Rauch, M. 2011, *The Astronomer's Telegram*, 3143, 1
- Uemura, M., Kato, T., Matsumoto, K., et al. 2000, *PASJ*, 52, L15
- Whitehurst, R., & King, A. 1991, *MNRAS*, 249, 25
- White, N. E., & Angelini, L. 2001, *ApJ*, 561, L101
- Younes, G., Boirin, L., & Sabra, B. 2009, *A&A*, 502, 905
- Zurita, C., Casares, J., Shahbaz, T., et al. 2002, *MNRAS*, 333, 791
- Zurita, C., Torres, M. A. P., Steeghs, D., et al. 2006, *ApJ*, 644, 432
- Zurita, C., Durant, M., Torres, M. A. P., et al. 2008, *ApJ*, 681, 1458



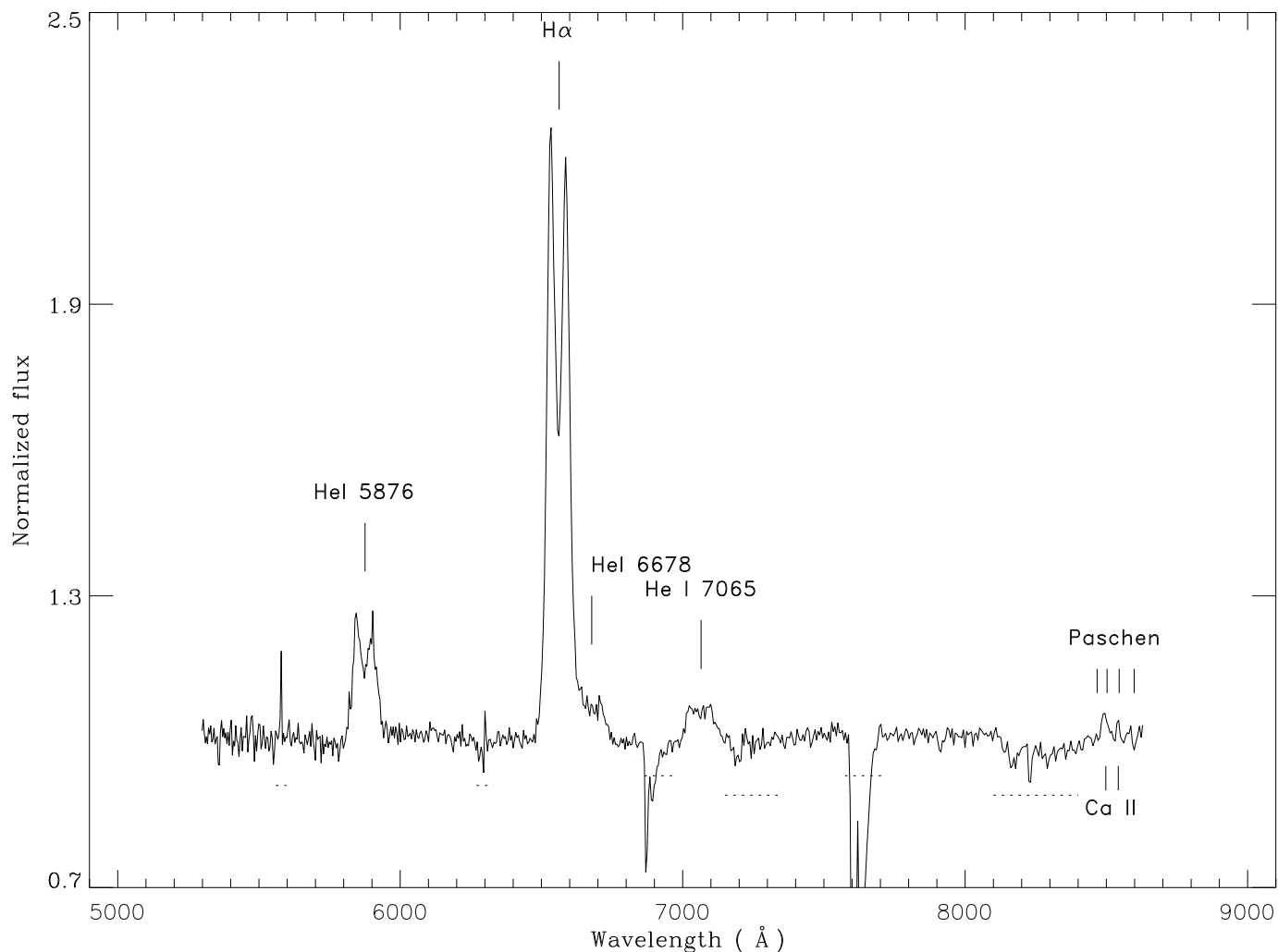


**Figure 1.** Continuum-normalized and averaged optical spectrum of J1357.2 in quiescence. The rest wavelengths for  $H\alpha$  and identified He I disc line are provided. For the sake of clarity, we also mark the rest wavelengths for the two Ca II infrared components at  $\lambda\lambda 8498, 8542$  and Paschen lines at  $\lambda\lambda 8467, 8502, 8545, 8598$ . The dashed lines below the source continuum mark the location of strong telluric features and residual sky emission lines.

**Table 1.** Emission line parameters: Centroid and peak-to-peak separation ( $\Delta V^{PP}$ ) derived from a 2-Gaussian fit to the line profiles (except for He I  $\lambda 7065$  where the line was fit with a single Gaussian). The FWHM was derived from a single Gaussian fit and corrected for the instrumental spectral resolution. The uncertainties for the centroid, peak-to-peak separation and FWHM were calculated after scaling the data error bars to yield a fit with  $\chi^2/d.o.f = 1$ . The uncertainties in the EWs are estimated by determining the scatter in the values derived when selecting different wavelength intervals to set the local continuum level. The FWZIs are given as lower limits since the ability to determinate the extension of the line wings is usually set by the signal-to-noise in the data.

	$H\alpha$	He I 5876	He I 7065
Centroid (km/s)	$-137 \pm 8$	$-180 \pm 40$	$-100 \pm 100$
$\Delta V^{PP}$ (km/s)	$2340 \pm 20$	$2640 \pm 70$	—
FWHM (km/s)	$4025 \pm 110$	$4500 \pm 200$	$4290 \pm 250$
FWZI (km/s)	$\gtrsim 6300$	$\gtrsim 7040$	$\gtrsim 5900$
EW (Å)	$-92 \pm 1$	$-19 \pm 1$	$-9 \pm 2$

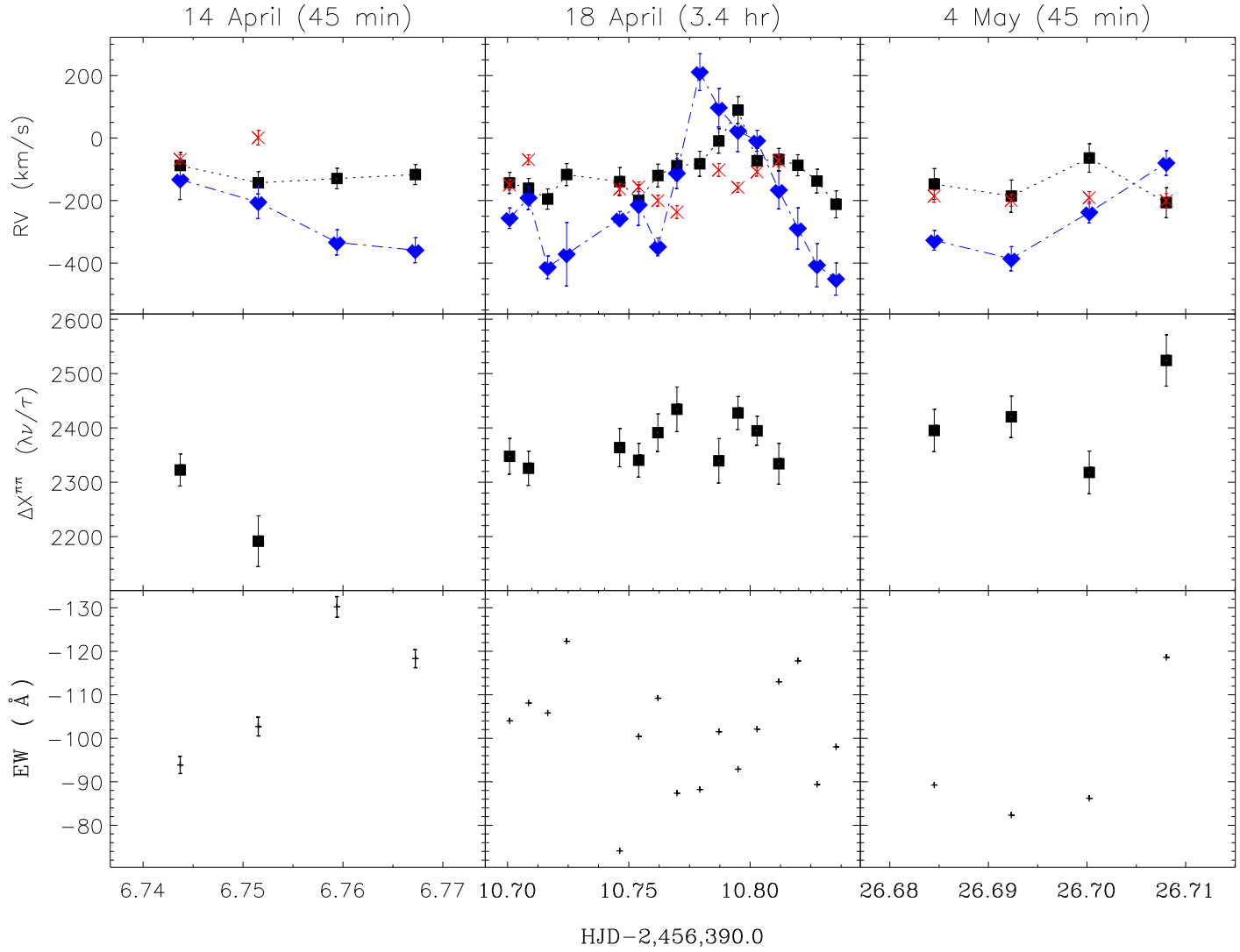


**Figure 2.**  $H\alpha$  emission line variability over the three nights of observations. Top: radial velocities from a single Gaussian fit (■) and the double-Gaussian technique (◆). The line centroid derived with a 2-Gaussian model is also shown (X). Middle: peak-to-peak separation ( $\Delta V^{pp}$ ) from the 2-Gaussian model. Bottom: EW measured in the interval  $\lambda\lambda 6460 - 6650$ .

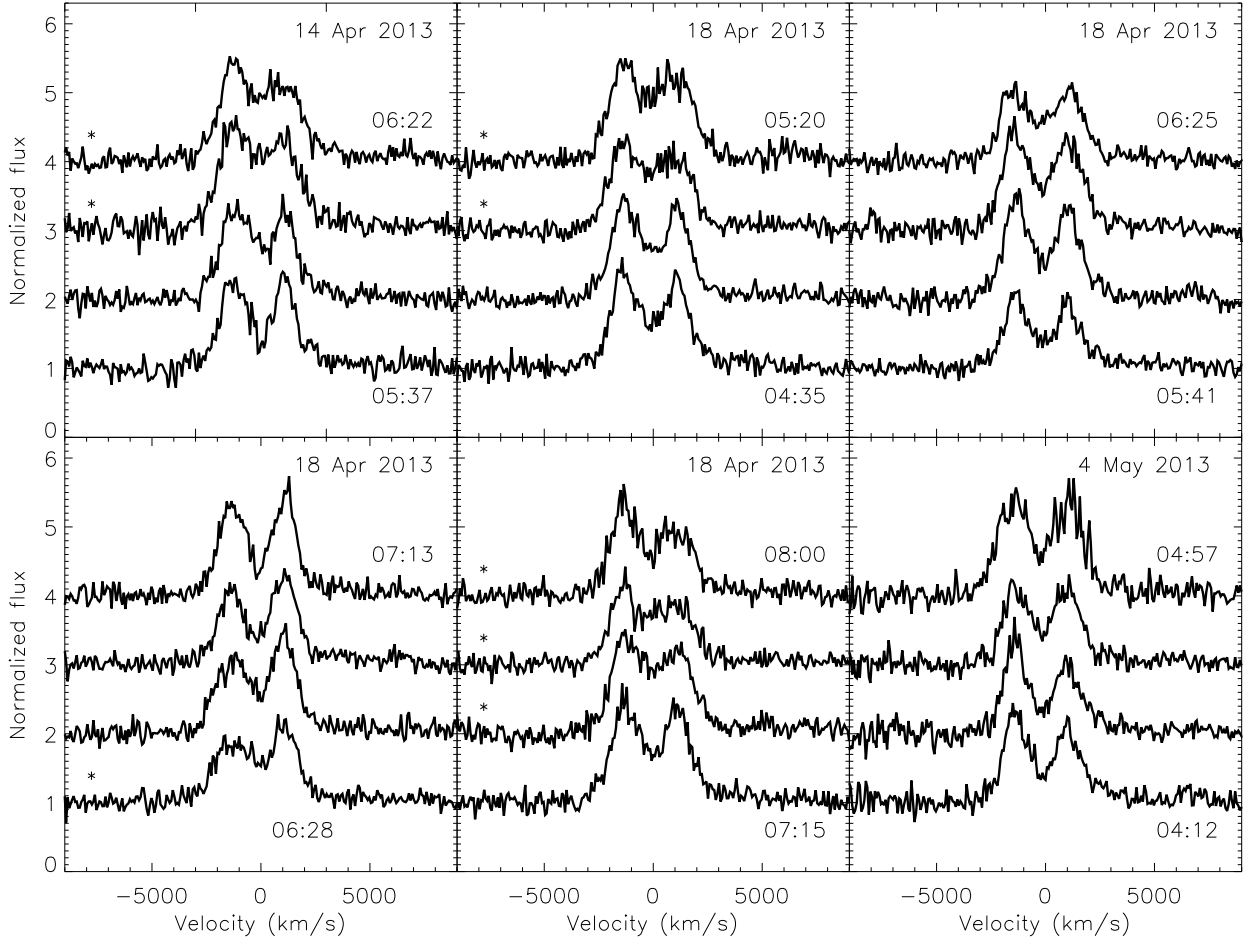


**Figure 3.** The 24 individual H $\alpha$  line profiles covering different observing times. For the sake of clarity each consecutive spectrum has been offset in the Y-direction. The starting and ending UT times of the spectroscopy obtained in the same observing block are given in each panel. Note the changes in the depth of the absorption component in the line center. An \* marks the eight asymmetric profiles discussed in Section 3.2.